Wave Motion 112 (2022) 102922

Contents lists available at ScienceDirect

Wave Motion

journal homepage: www.elsevier.com/locate/wamot

Interfacial wave between acoustic media with Willis coupling

Zhanyu Li, Hongfei Qu, Hongkuan Zhang, Xiaoning Liu, Gengkai Hu *

School of Aerospace Engineering, Beijing Institute of Technology, Beijing, 100081, China

ARTICLE INFO

Article history:
Received 9 April 2021
Received in revised form 24 July 2021
Accepted 1 March 2022
Available online 6 May 2022

Keywords:
Interfacial wave
Metamaterial
Acoustic Willis material
Bianisotropy
Willis coupling
Wave control

ABSTRACT

Acoustic Willis materials, also known as acoustic bianisotropic materials, exhibit unconventional coupling between pressure and velocity, as well as momentum and strain, which have been shown to enable extraordinary control over the propagation of acoustic waves. Our work first predicts that, under proper conditions, interfacial mode can exist at the interface between two acoustic Willis materials, and the existence of the interfacial wave strongly relies on relative orientations of the Willis coupling vectors of the two materials. To demonstrate our theory, experiments are also conducted utilizing a well-designed adjustable acoustic Willis metamaterial. Our experimental results are in good agreement with simulation and theoretical analysis, although there is unavoidable acoustic attenuation in experiments due to damping effect. This work presents a new functional design with acoustic Willis materials and opens a new route to control acoustic waves.

1. Introduction

Metamaterials are composite materials constructed with artificially designed microstructures, which has dramatically enlarged the range of material properties in many systems, including electromagnetism [1–4], thermodynamics [5] and elastodynamics [6–8]. In the context of acoustics, unconventional properties such as negative bulk modulus [9,10], negative or anisotropic mass density [7,11,12], negative or zero refractive index [13,14] have now been realized, enabling abundant wave control applications, such as negative refraction [15,16], superlensing [17,18] and acoustic cloaking [19,20]. Notably, Willis materials, initially proposed by J. R. Willis [21] and further revisited by many researchers theoretically [22,23] and experimentally [24], as an elastic/acoustic analogy of bianisotropy in electromagnetism, have greatly extended the capabilities of elastic/acoustic metamaterials. By introducing coupling between pressure and velocity, as well as momentum and volumetric strain, acoustic Willis materials have enabled exotic wave phenomena, e.g., the separate control of reflected and transmitted waves by using bianisotropic metasurfaces [25–28]. Besides, active elements have been utilized to design Willis meta-atoms with asymmetric scattering polarizabilities [29,30], which enable nonreciprocal operations.

Despite the great progress achieved so far, most of the recent research on acoustic Willis coupling is limited to the functional design of Willis meta-atoms or Willis metasurfaces, and the full potential of acoustic Willis materials remains to be achieved. In this work, we propose a novel function of acoustic Willis materials when there is an interface and demonstrate it experimentally. It is known [31] that, at the surface of solids, there can exist Rayleigh waves propagating along the surface, whose amplitude decreases exponentially with distance from the surface. There also exist Stoneley waves [32] that propagate along solid–solid interfaces and Scholte waves [33] that propagate along fluid–solid interfaces.

* Corresponding author.
E-mail address: hugeng@bit.edu.cn (G. Hu).

https://doi.org/10.1016/j.wavemoti.2022.102922
0165-2125/

As for fluid–fluid interfaces, researchers have recently discovered that there can exist a Rayleigh-type interfacial wave [34] between an ordinary acoustic fluid and a double negative acoustic fluid, i.e., a fluid with simultaneously negative density and negative bulk modulus. There are also discussions on the existence of interfacial wave between two fluids when at least one displays Willis coupling [35]. Inspired by these precursors, this paper demonstrates both theoretically and experimentally that, under certain conditions, interfacial wave mode, which is absent within ordinary acoustic fluids, can exist between two acoustic Willis materials, providing that their Willis coupling coefficients are patterned appropriately. This phenomenon may offer a new route to control acoustic waves.

This paper is structured as follows. In Section 2, acoustic Willis constitutive model is introduced and the conditions for the existence of interfacial mode are presented. In Section 3, firstly, a Willis metamaterial with artificial microstructure is designed, whose Willis coupling coefficients are adjustable. Then, by using the designed Willis metamaterial, an experiment is conducted to demonstrate the existence of interfacial mode. Finally, conclusions are presented in Section 4.

2. Homogeneous acoustic Willis material and interfacial mode

2.1. Acoustic Willis constitutive model

For a linear Cauchy acoustic material, acoustic pressure is determined by volumetric strain via bulk modulus and momentum density is determined by velocity via mass density. It is known that acoustic metamaterials extend the material density from a scalar to a tensor, allowing anisotropic density. For acoustic Willis materials, extra coupling exists between pressure and velocity, as well as momentum density and volumetric strain, via Willis coupling coefficients. In frequency domain, the constitutive equations of acoustic Willis materials are [36]

$$\begin{cases} -p = \kappa \varepsilon_V + \boldsymbol{s} \cdot \boldsymbol{v}, \\ \boldsymbol{\mu} = \tilde{\boldsymbol{s}} \varepsilon_V + \boldsymbol{\rho} \cdot \boldsymbol{v}, \end{cases} \tag{1}$$

where p, $\boldsymbol{\mu}$, ε_V and $\boldsymbol{v}$ represent, respectively, acoustic pressure, momentum density, volumetric strain and particle velocity. κ is bulk modulus, $\boldsymbol{\rho}$ is mass density tensor of order two, and $\boldsymbol{s}$ and $\tilde{\boldsymbol{s}}$ are the Willis coupling coefficients in vector form. The equation of motion without external force is

$$-\nabla p = \dot{\boldsymbol{\mu}}. \tag{2}$$

Note that all the quantities and results in this paper are expressed in frequency domain ($e^{-i\omega t}$ is assumed, where ω is angular frequency), and nonlocal effects of Willis materials are neglected. Therefore, for a homogeneous material, the material parameters κ, $\boldsymbol{\rho}$, $\boldsymbol{s}$ and $\tilde{\boldsymbol{s}}$ in Eqs. (1) and (2) are functions of ω only. It has been proven that, under the constraint of reciprocity and passivity and in linear lossless media, κ and $\boldsymbol{\rho}$ should be real, while $\boldsymbol{s}$ and $\tilde{\boldsymbol{s}}$ should be purely imaginary [36]. In addition, the following relations must be satisfied:

$$\boldsymbol{\rho} = \boldsymbol{\rho}^{\mathrm{T}}, \quad \boldsymbol{s} = \tilde{\boldsymbol{s}}. \tag{3}$$

Sometimes, it is more convenient to use the inverse relation of Eq. (1) as follows:

$$\begin{cases} \varepsilon_V = -\gamma p + \boldsymbol{g} \cdot \boldsymbol{\mu}, \\ \boldsymbol{v} = -\boldsymbol{g} p + \boldsymbol{a} \cdot \boldsymbol{\mu}, \end{cases} \tag{4}$$

and the material parameters in Eq. (4) are determined by

$$\begin{cases} \gamma = \left(\kappa - \boldsymbol{s} \cdot \boldsymbol{\rho}^{-1} \cdot \boldsymbol{s}\right)^{-1}, \\ \boldsymbol{g} = -\gamma \boldsymbol{\rho}^{-1} \cdot \boldsymbol{s}, \\ \boldsymbol{a} = \boldsymbol{\rho}^{-1} + \gamma^{-1} \boldsymbol{g} \otimes \boldsymbol{g}. \end{cases} \tag{5}$$

Substituting a plane wave form ($p \propto \exp\left[i(\boldsymbol{k} \cdot \boldsymbol{x} - \omega t)\right]$) into Eqs. (2) and (4), we can get the dispersion relation of a homogeneous acoustic Willis material as

$$\gamma \omega^2 = \boldsymbol{k} \cdot \boldsymbol{a} \cdot \boldsymbol{k}, \tag{6}$$

which is also given in an equivalent form in Ref. [37]. In general, in the presence of nonzero Willis coupling vector $\boldsymbol{s}$, the equifrequency curve of an acoustic Willis material is an ellipse even the density tensor is isotropic, showing obvious directionality.

2.2. Conditions for interfacial mode

In this section, we will prove that, under certain conditions, interfacial mode may appear at the interface between two different acoustic Willis materials. The conditions for the existence of interfacial mode will be firstly derived.

As shown in Fig. 1(a), the problem studied here concerns an interface at $x = 0$ separating two different semi-infinite homogeneous acoustic Willis materials. The material at $x < 0$ is denoted by medium 1 with material parameters of $\gamma^{(1)}$,

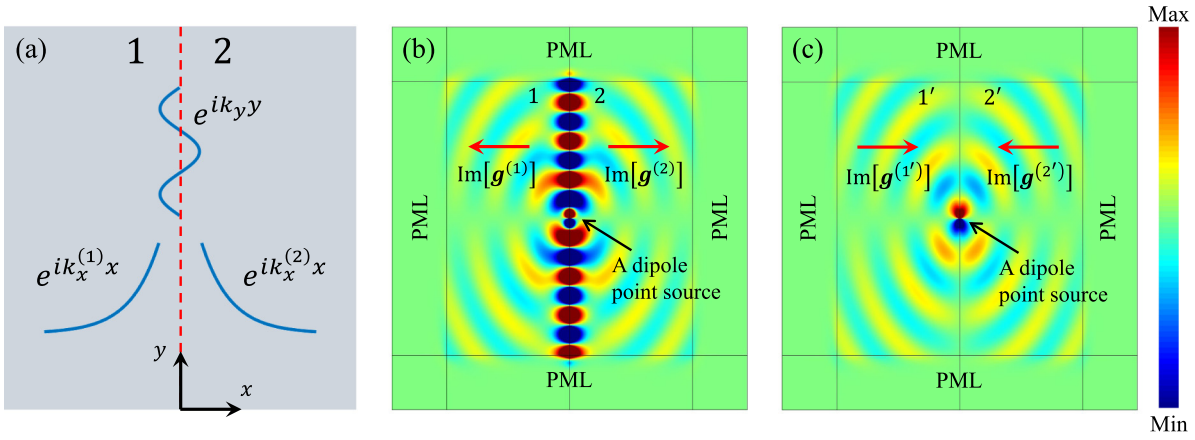

Fig. 1. (a) The schematic of interfacial mode at an interface (red dotted line) separating two semi-infinite homogeneous acoustic Willis materials. The blue lines represent traveling wave along the interface and evanescent waves normal to the interface; (b) Simulation results of the interfacial wave. The media 1 and 2 are homogeneous acoustic Willis materials with isotropic density. $\kappa^{(1)} = \kappa^{(2)} > 0$, $\rho^{(1)} = \rho^{(2)} > 0$ and $\boldsymbol{s}^{(1)}/\sqrt{\kappa^{(1)}\rho^{(1)}} = -\boldsymbol{s}^{(2)}/\sqrt{\kappa^{(2)}\rho^{(2)}} = [i, 0]^{\mathrm{T}}$. A dipole point source oscillating along y axis is located at the interface; (c) Simulation results when the media 1 and 2 are exchanged. In this case, interfacial wave no longer exists.

$\boldsymbol{g}^{(1)}$ and $\boldsymbol{a}^{(1)}$, while the material at $x > 0$ is denoted by medium 2 with material parameters of $\gamma^{(2)}$, $\boldsymbol{g}^{(2)}$ and $\boldsymbol{a}^{(2)}$. Note that, in this paper, the superscript (1) represents quantities of the medium 1, and the superscript (2) represents quantities of the medium 2.

If an interfacial wave exists, the acoustic pressure fields on the two sides should be expressed as

$$p^{(1)} = Pe^{ik_x^{(1)}x}e^{ik_y y} \tag{7}$$

for the medium 1, and

$$p^{(2)} = Pe^{ik_x^{(2)}x}e^{ik_y y} \tag{8}$$

for the medium 2, where P is the complex pressure amplitude of the interfacial wave, $k_x^{(1)}$ and $k_x^{(2)}$ are the components of wave vector normal to the interface in the media 1 and 2, respectively, and k_y is the component of wave vector parallel to the interface. It is worth noting that $k_x^{(1)}$ and k_y should satisfy the dispersion relation given by Eq. (6), and so should $k_x^{(2)}$ and k_y as well. Since the interfacial wave is propagating along the interface, k_y should satisfy $\mathrm{Re}\, k_y \neq 0$ and $\mathrm{Im}\, k_y = 0$ for lossless media. On the other hand, since the interfacial wave is evanescent in the direction normal to the interface, $k_x^{(1)}$ and $k_x^{(2)}$ should satisfy

$$\mathrm{Im}\left[k_x^{(1)}\right] < 0, \quad \mathrm{Im}\left[k_x^{(2)}\right] > 0. \tag{9}$$

It is obvious that Eqs. (7) and (8) ensure the continuity of pressure at the interface. The continuity of normal velocity at the interface requires

$$v_x^{(1)}\big|_{x=0} = v_x^{(2)}\big|_{x=0}. \tag{10}$$

By using Eq. (4), the above equation can be written in component form as

$$-g_x^{(1)} + \frac{1}{\omega}\left[a_{xx}^{(1)}k_x^{(1)} + a_{xy}^{(1)}k_y\right] = -g_x^{(2)} + \frac{1}{\omega}\left[a_{xx}^{(2)}k_x^{(2)} + a_{xy}^{(2)}k_y\right]. \tag{11}$$

Therefore, Eqs. (6), (9) and (11) provide the conditions for the existence of interfacial mode. For simplicity, in this paper we only consider the situation when the media 1 and 2 are mirror symmetric about y axis. Based on this assumption, the material parameters of the media 1 and 2 satisfy the following relations:

$$\begin{aligned} &\gamma^{(1)} = \gamma^{(2)}, \quad \boldsymbol{g}^{(1)} = \begin{bmatrix} g_x^{(1)} \\ g_y^{(1)} \end{bmatrix}, \quad \boldsymbol{g}^{(2)} = \begin{bmatrix} g_x^{(2)} \\ g_y^{(2)} \end{bmatrix} = \begin{bmatrix} -g_x^{(1)} \\ g_y^{(1)} \end{bmatrix}, \\ &\boldsymbol{a}^{(1)} = \begin{bmatrix} a_{xx}^{(1)} & a_{xy}^{(1)} \\ a_{xy}^{(1)} & a_{yy}^{(1)} \end{bmatrix}, \quad \boldsymbol{a}^{(2)} = \begin{bmatrix} a_{xx}^{(2)} & a_{xy}^{(2)} \\ a_{xy}^{(2)} & a_{yy}^{(2)} \end{bmatrix} = \begin{bmatrix} a_{xx}^{(1)} & -a_{xy}^{(1)} \\ -a_{xy}^{(1)} & a_{yy}^{(1)} \end{bmatrix}. \end{aligned} \tag{12}$$

And the wavenumbers along x axis satisfy $k_x^{(1)} = -k_x^{(2)}$. Therefore, Eq. (11) can be simplified as

$$\omega g_x^{(1)} = a_{xx}^{(1)}k_x^{(1)} + a_{xy}^{(1)}k_y. \tag{13}$$

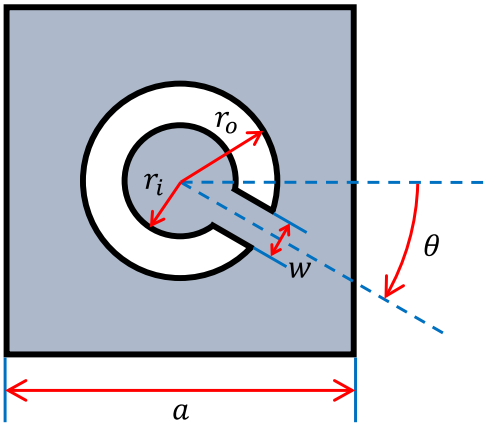

Fig. 2. Schematic of the designed unit cell.

Using Eqs. (9) and (13), the following three conditions for the existence of interfacial wave can be derived,

$$\begin{aligned}
&\text{cond. 1:} && \frac{\mathrm{Im}\left[g_x^{(1)}\right]}{\mathrm{sgn}\left[a_{xx}^{(1)}\right]} < 0, \quad a_{xx}^{(1)}a_{yy}^{(1)} - \left[a_{xy}^{(1)}\right]^2 > 0 \quad \text{and} \quad a_{xx}^{(1)}\gamma^{(1)} \geq 0; \\
&\text{cond. 2:} && \frac{\mathrm{Im}\left[g_x^{(1)}\right]}{\mathrm{sgn}\left[a_{xx}^{(1)}\right]} \leq -\sqrt{-a_{xx}^{(1)}\gamma^{(1)}}, \quad a_{xx}^{(1)}a_{yy}^{(1)} - \left[a_{xy}^{(1)}\right]^2 > 0 \quad \text{and} \quad a_{xx}^{(1)}\gamma^{(1)} < 0; \\
&\text{cond. 3:} && -\sqrt{-a_{xx}^{(1)}\gamma^{(1)}} \leq \frac{\mathrm{Im}\left[g_x^{(1)}\right]}{\mathrm{sgn}\left[a_{xx}^{(1)}\right]} < 0, \quad a_{xx}^{(1)}a_{yy}^{(1)} - \left[a_{xy}^{(1)}\right]^2 < 0 \quad \text{and} \quad a_{xx}^{(1)}\gamma^{(1)} < 0,
\end{aligned} \tag{14}$$

where sgn(•) denotes the sign function.

Fig. 1(b) shows an example of numerical simulation of the interfacial wave, calculated by commercially available software COMSOL. The media 1 and 2 are homogeneous acoustic Willis materials with the same positive bulk modulus and the same positive isotropic density, i.e., $\kappa^{(1)} = \kappa^{(2)} > 0$ and $\rho^{(1)} = \rho^{(2)} > 0$. The Willis coupling vectors of the two media are mirror symmetric about y axis, expressed as $\boldsymbol{s}^{(1)}/\sqrt{\kappa\rho} = -\boldsymbol{s}^{(2)}/\sqrt{\kappa\rho} = [i, 0]^{\mathrm{T}}$. By using Eq. (5), it can be easily obtained that $g_x^{(1)} = -g_x^{(2)} = -i/(2\sqrt{\kappa\rho})$ and $a_{xx}^{(1)} = a_{xx}^{(2)} = (2\rho)^{-1} > 0$, which satisfy the condition 1 for the existence of interfacial wave given by Eqs. (14). A dipole point source polarized along y axis is located at the interface. Furthermore, a custom perfectly matched layer for acoustic Willis materials is developed based on the theory of complex coordinate transformation acoustics [38,39]. As shown in Fig. 1(b), an obvious wave channel is observed along the interface and decays away from the interface, confirming the theoretical prediction. In contrast, Fig. 1(c) shows the result of the same setup except that the media 1 and 2 are exchanged. In this case, the conditions given by Eqs. (14) for the existence of interfacial mode are not satisfied, and it is seen that no interfacial mode can be excited out as expected.

Furthermore, since acoustic symmetric boundary is equivalent to acoustic hard boundary in mathematics, it is directly deduced that surface waves can exist at sound hard boundaries of acoustic Willis materials. It is also interesting to explore surface waves of Willis materials in other cases, which is not the objective of the current study.

3. Microstructural design and experimental validation

3.1. Metamaterial model and effective properties based on retrieval method

To realize the above-mentioned interfacial mode, an adjustable locally resonant acoustic Willis metamaterial, initially proposed by Melnikov et al. [40], is adopted. As shown in Fig. 2, the designed unit cell consists of a C-shaped Helmholtz resonator, which is non-centrosymmetric in order to increase the Willis coupling. The orientation angle θ of the slit of the Helmholtz resonator is adjustable to obtain different Willis coupling vector $\boldsymbol{s}$. The geometrical parameters of the microstructure are listed in Table 1. The wall of the Helmholtz resonator is modeled as acoustic rigid boundary, and the background medium is air (density = 1.205 kg/m^3 and sound speed = 343 m/s). The unit cells are periodically arranged in square lattice, and the band structures of the metamaterial when $\theta = 0°$ and $\theta = 45°$ are shown in Figs. 3(a) and 3(e) respectively. It can be seen that a band gap exists in the frequency range of around 4700 ∼ 5000 Hz in these cases. It is

Table 1
Unit cell geometry of the Willis acoustic medium.

Geometrical properties	Description	Quantity
a	Lattice constant (square lattice)	25 mm
r_o	Outer radius of the resonant cavity	7 mm
r_i	Inner radius of the resonant cavity	4 mm
w	Width of the slit of the resonant cavity	3 mm
θ	Orientation angle of the slit of the resonant cavity	$0 \sim 360°$

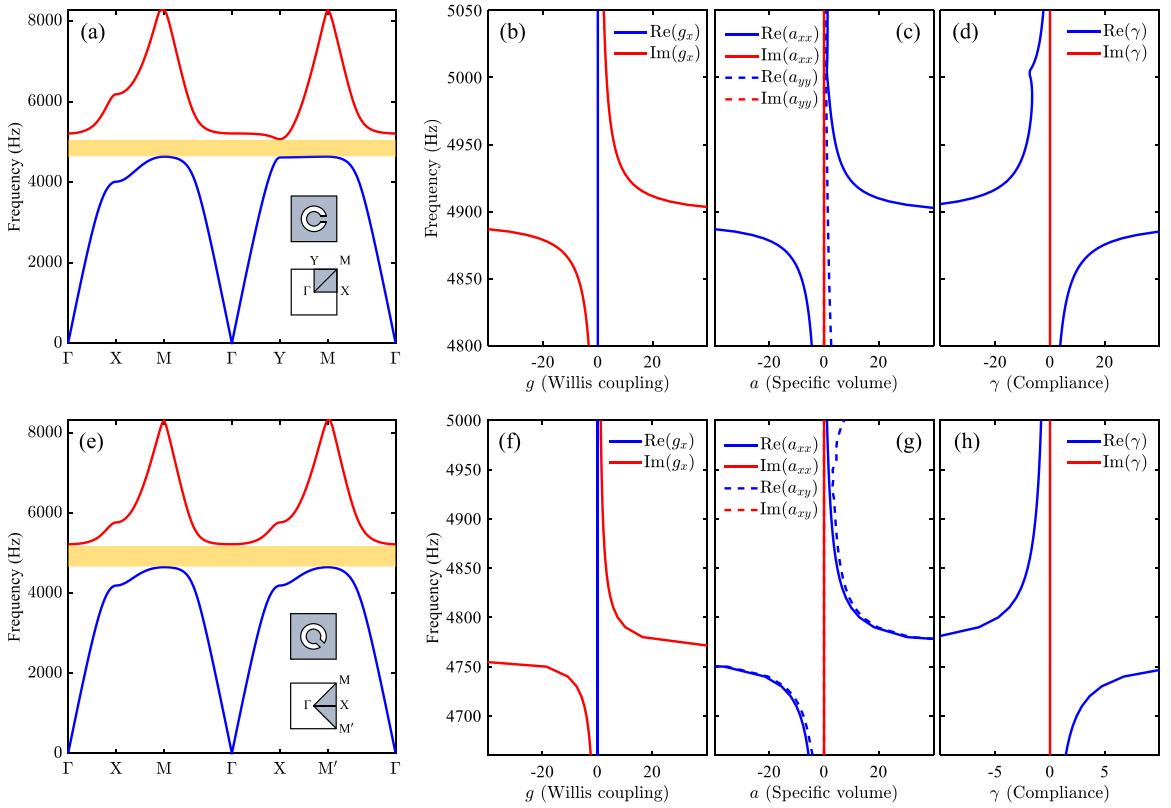

Fig. 3. (a) Band structure of the metamaterial when $\theta = 0°$; (b–d) The plots of retrieved nondimensionalized effective properties $\boldsymbol{g}$, $\boldsymbol{a}$ and γ with respect to frequencies among 4800 $\sim$ 5050 Hz when $\theta = 0°$. In this case, $g_y = 0$ and $a_{xy} = 0$ due to symmetry. Note that the plotted effective properties are nondimensionalized based on the properties of air, as $\rho_{\text{air}} c_{\text{air}} \boldsymbol{g}$, $\rho_{\text{air}} \boldsymbol{a}$ and $\rho_{\text{air}} c_{\text{air}}^2 \gamma$ respectively; (e) Band structure of the metamaterial when $\theta = 45°$; (f–h) The plots of retrieved nondimensionalized effective properties $\boldsymbol{g}$, $\boldsymbol{a}$ and γ with respect to frequencies among 4660 $\sim$ 5000 Hz when $\theta = 45°$. In this case, $g_y = -g_x$ and $a_{yy} = a_{xx}$ due to symmetry.

found, based on the retrieval method [24], that the metamaterial possesses strong Willis coupling in this band gap (see Figs. 3(b) and 3(f)), due to both the non-centrosymmetric microstructure and locally resonant effects. It is worth noting here that this kind of anisotropy reflecting the orientation of the Helmholtz resonator cannot be distinguished when the metamaterial is homogenized to an ordinary acoustic medium, particularly near the resonant frequency of the Helmholtz resonator, indicating the necessity of introducing Willis coupling.

In what follows, we will determine the effective properties of the metamaterial in the band gap. Since the disturbance of body wave vanishes in the band gap, so we can control the acoustic wave to propagate only along the interface.

The effective parameters of the metamaterial are retrieved from the reflection and transmission coefficients computed by finite element method (FEM). The retrieval method in this paper is based on the method for 1-dimensional acoustic Willis materials as in Ref. [24]. At a given frequency, the reflection and transmission coefficients of the 2D acoustic Willis metamaterial are computed in a series of directions, and the constitutive parameters are retrieved from these coefficients. Here, effective medium theory is assumed to be valid since the unit cell size is small compared to wavelength.

Fig. 3(b–d, f–h) show plots of the retrieved nondimensionalized effective properties $\boldsymbol{g}$, $\boldsymbol{a}$ and γ of the metamaterial as a function of frequency for orientation angles $\theta = 0°$ and $\theta = 45°$. It can be seen that the Willis coupling coefficients depend strongly on θ. Based on these results, the effective properties when $\theta = 180°$ and $\theta = 135°$ can be obtained easily due to the mirror symmetry of these cases. The effective properties for two mirror-symmetric orientation angles θ

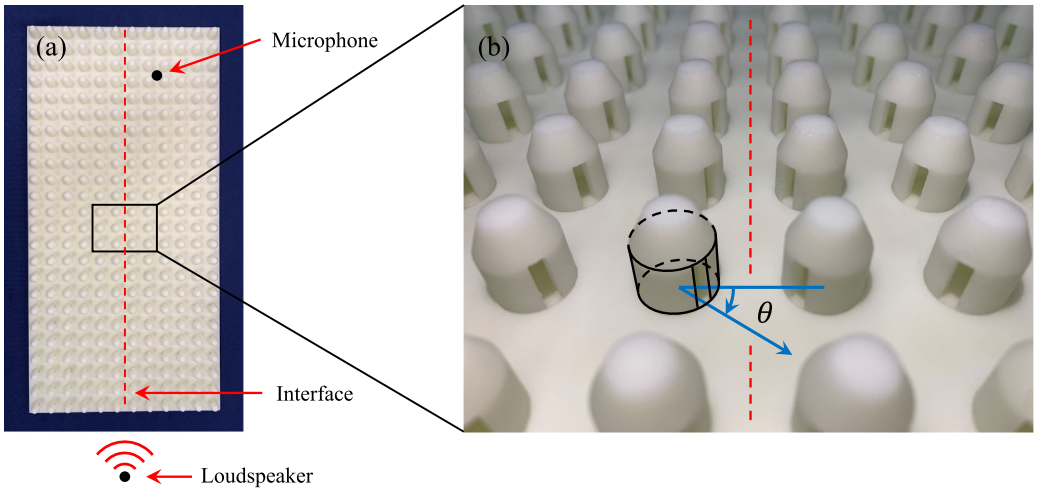

Fig. 4. (a) Schematic of experimental set-up used to demonstrate the existence of the interfacial wave. The designed 2D slab waveguide (300 mm length, 600 mm height) consists of 12 × 24 unit cells. The red dotted line represents the interface of two different acoustic Willis materials; (b) The detailed view that shows the microstructure of unit cells and the orientation angle θ of C-shaped Helmholtz resonator.

and θ' via y axis ($\theta + \theta' = 180°$) should satisfy

$$\begin{cases} \gamma = \gamma', \\ g_x = -g_x', \quad g_y = g_y', \\ a_{xx} = a_{xx}', \quad a_{xy} = -a_{xy}', \quad a_{yy} = a_{yy}', \end{cases} \tag{15}$$

where the superscript prime represents the effective properties for θ'. Therefore, we can design acoustic Willis metamaterials with different Willis coupling coefficients by adjusting orientation angle θ.

3.2. Simulations and experiments

To demonstrate the existence of the interfacial wave as predicted by our theory, experimental validation is carried out. A 2D slab waveguide (thickness = 10 mm) is designed and fabricated, consisting of 12 × 24 unit cells (C-shaped Helmholtz resonator) and an interface at the center. The front view and detailed side view of the sample are shown in Fig. 4(a) and 4(b) respectively. The geometrical parameters of the unit cell are given in Table 1. The orientation angle θ of resonant cavities can be easily adjusted to examine the influence of Willis coupling on the interfacial wave.

For convenience, all experimental samples, containing two cover plates of the 2D waveguide and 12 × 24 internal periodically arranged Helmholtz resonators, are fabricated by 3D printing using stereolithography apparatus (SLA) technique, and the base material is photopolymer with density of 1.1×10^3 kg/m^3 and Young's modulus of 2.6 GPa. Since the acoustic impedance of photopolymer is much greater than air, it is reasonable to consider the photopolymer structure rigid. The experimental samples are properly designed so that the two cover plates and the resonant cavities can be assembled together, and a slot for each resonant cavity is designed so that its orientation can be precisely adjusted and fixed.

The principle of the experimental set-up is shown in Fig. 4(a), with the interface of the two materials oriented along the midline of the waveguide. A loudspeaker is fixed to one end of the interface, and a microphone is fixed to a 2D guide rail by a thin bar, which allows precisely controlling the position of the microphone by a LabVIEW program. During the experiment, the microphone is carried to the target point by the 2D rail, and subsequently the loudspeaker emits a Gaussian-modulated sinusoidal wave packet with a center frequency of 4800 Hz, then the internal acoustic pressure signal at the target point is measured by the microphone and recorded by NI PXIe data acquisition and processing system. Repeating the process, the pressure field at the interspace among these resonant cavities can be measured. Finally, by using Fourier transform, the measured signals in time domain are transformed into frequency domain, and the amplitude and phase of the acoustic wave in the frequency range of 4500 ∼ 5100 Hz are retrieved. As a result, the pressure field in a rectangular region of 300 mm × 600 mm is scanned with a step size of 25 mm.

The simulation results and the corresponding experimental results are shown in Fig. 5 with different orientation angles of the resonant cavities on both sides. The simulation results are calculated by FEM using commercial software COMSOL. The operation frequency is chosen at 4950 Hz. When the slits of Helmholtz resonators on both sides are back-to-back as shown in Figs. 5(a–c, g–i), the conditions for the existence of interfacial mode, expressed by Eqs. (14), are satisfied. Therefore, interfacial wave exists in these cases. On the contrary, when the slits of Helmholtz resonators on both sides

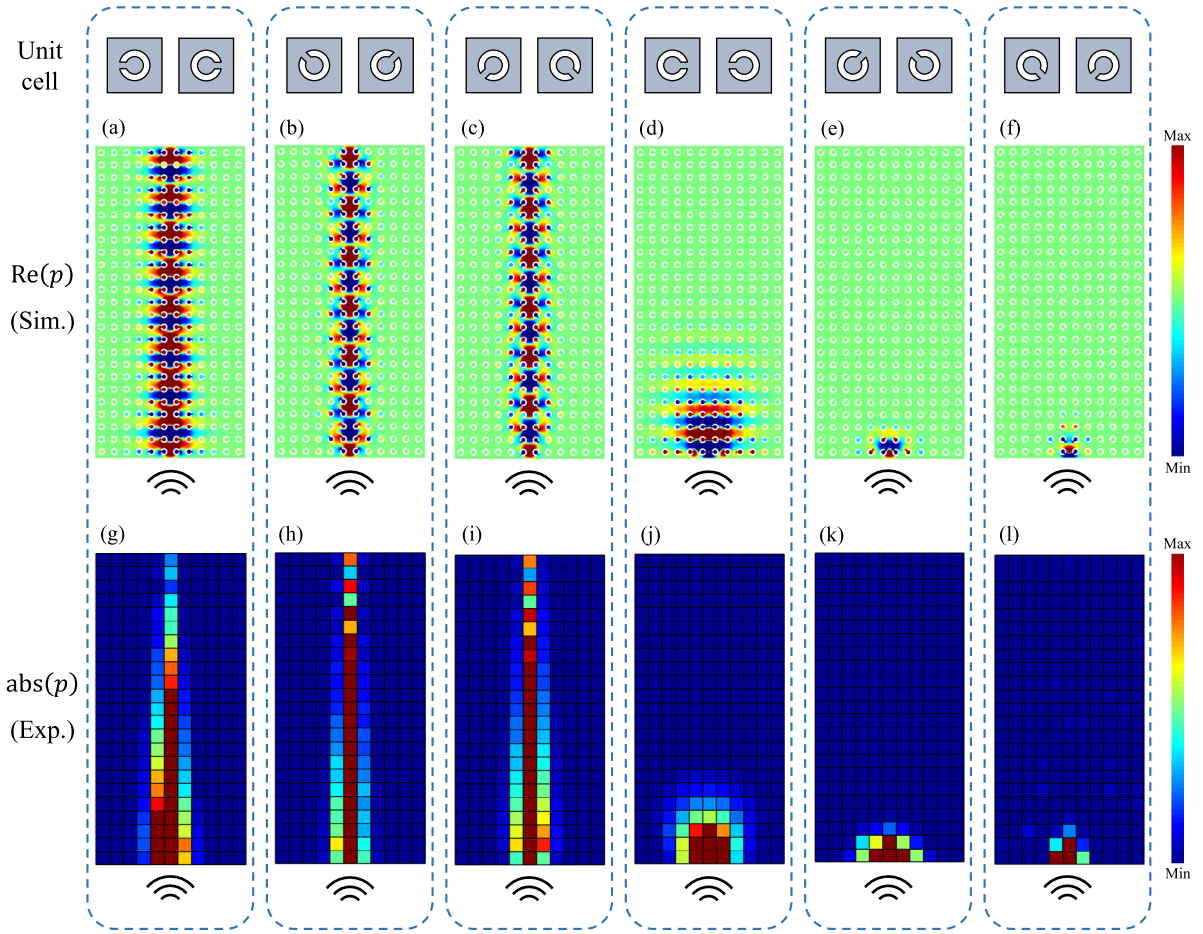

Fig. 5. Simulation and experimental results with different orientation angles of the Helmholtz resonators. (a–f) Simulation results. The real part of acoustic pressure is plotted; (g–l) experimental results. The amplitude of acoustic pressure is plotted; The orientation angles of medium 1 are (a, g) $\theta^{(1)} = 180°$, (b, h) $\theta^{(1)} = -135°$, (c, i) $\theta^{(1)} = 135°$, (d, j) $\theta^{(1)} = 0°$, (e, k) $\theta^{(1)} = -45°$, and (f, l) $\theta^{(1)} = 45°$, respectively. The corresponding orientation angles of medium 2 are obtained by mirror symmetry. Operation frequency is 4950 Hz, for all cases.

are face-to-face as shown in Figs. 5(d–f, j–l), Eqs. (14) are not satisfied, and therefore interfacial wave vanishes in these cases. Since the operation frequency 4950 Hz is in the band gap of the metamaterials on both sides, body wave is not supported, which allows a clear observation of interfacial wave.

For a better understanding, a typical interfacial mode shape plotted by velocity fields is shown in Fig. 6. The operation frequency is 4950 Hz and the orientation angle $\theta^{(1)}$ of the resonators of medium 1 is $\theta^{(1)} = 180°$, which corresponds to the case in Fig. 5(a). The interfacial mode shape is calculated numerically by Bloch analysis of a supercell, and only the region near the interface is shown in Fig. 6. The wavenumber k_y is chosen to be positive, and the interfacial wave propagates upwards along the interface. It can be seen that, at the interface, the velocity component normal to the interface vanishes. Therefore, if the medium 2 is replaced by a rigid wall, then the pressure and velocity fields in medium 1 do not change, i.e., the interfacial wave changes to a surface wave. This is an intuitive explanation of the existence of surface waves at sound hard boundaries of acoustic Willis materials.

4. Conclusion

In summary, this paper provides a theoretical and experimental study on the interfacial mode supported by an interface between two acoustic Willis materials. We for the first time predict that interfacial mode can exist on the interface between two acoustic Willis materials and provide the corresponding conditions. Our theoretical predictions are experimentally demonstrated utilizing Willis metamaterials with well-designed microstructure, and experimental results are in good agreement with numerical simulations. Our findings present a new progress in passive acoustic system with Willis coupling, which paves the way to design future acoustic wave control devices.

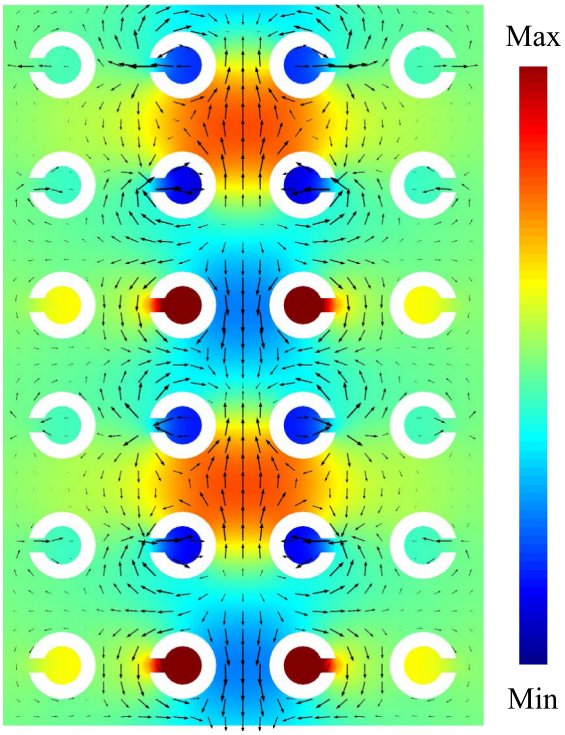

Fig. 6. Numerically calculated interfacial mode shapes plotted by velocity fields at 4950 Hz with the orientation angle $\theta^{(1)} = 180°$. The interfacial wave propagates upwards with a wavenumber $k_y = 0.6703\pi/a$.

CRediT authorship contribution statement

Zhanyu Li: Conceptualization, Methodology, Software, Investigation, Writing – original draft, Writing – review & editing, Visualization. **Hongfei Qu:** Conceptualization, Software, Validation. **Hongkuan Zhang:** Data curation, Investigation, Formal analysis, Visualization. **Xiaoning Liu:** Resources, Supervision, Project administration, Funding acquisition. **Gengkai Hu:** Resources, Supervision, Project administration, Funding acquisition.

Declaration of competing interest

The authors declare that they have no known competing financial interests or personal relationships that could have appeared to influence the work reported in this paper.

Acknowledgments

We thank the support of National Natural Science Foundation of China (Grants No. 11632003, No. 11972083, No. 11991030, No. 11972080).

References

[1] J. Pendry, A. Holden, D. Robbins, W. Stewart, Magnetism from conductors and enhanced nonlinear phenomena, IEEE Trans. Microw. Theory Tech. 47 (11) (1999) 2075–2084, http://dx.doi.org/10.1109/22.798002.

[2] D.R. Smith, W.J. Padilla, D.C. Vier, S.C. Nemat-Nasser, S. Schultz, Composite medium with simultaneously negative permeability and permittivity, Phys. Rev. Lett. 84 (2000) 4184–4187, http://dx.doi.org/10.1103/PhysRevLett.84.4184, URL https://link.aps.org/doi/10.1103/PhysRevLett.84.4184.

[3] R.A. Shelby, D.R. Smith, S. Schultz, Experimental verification of a negative index of refraction, Science 292 (5514) (2001) 77–79, http://dx.doi.org/10.1126/science.1058847, arXiv:https://science.sciencemag.org/content/292/5514/77.full.pdf, URL https://science.sciencemag.org/content/292/5514/77.

[4] J.B. Pendry, D. Schurig, D.R. Smith, Controlling electromagnetic fields, Science 312 (5781) (2006) 1780–1782, http://dx.doi.org/10.1126/science.1125907, arXiv:https://science.sciencemag.org/content/312/5781/1780.full.pdf, URL https://science.sciencemag.org/content/312/5781/1780.

[5] T. Han, X. Bai, J.T.L. Thong, B. Li, C.-W. Qiu, Full control and manipulation of heat signatures: Cloaking, camouflage and thermal metamaterials, Adv. Mater. 26 (11) (2014) 1731–1734, http://dx.doi.org/10.1002/adma.201304448, arXiv:https://onlinelibrary.wiley.com/doi/pdf/10.1002/adma.201304448, URL https://onlinelibrary.wiley.com/doi/abs/10.1002/adma.201304448.

[6] G.W. Milton, J.R. Willis, On modifications of Newton's second law and linear continuum elastodynamics, Proc. R. Soc. A Math. Phys. Eng. Sci. 463 (2079) (2007) 855–880, http://dx.doi.org/10.1098/rspa.2006.1795, arXiv:https://royalsocietypublishing.org/doi/pdf/10.1098/rspa.2006.1795, URL https://royalsocietypublishing.org/doi/abs/10.1098/rspa.2006.1795.

[7] S. Yao, X. Zhou, G. Hu, Experimental study on negative effective mass in a 1D mass–spring system, New J. Phys. 10 (4) (2008) 043020, http://dx.doi.org/10.1088/1367-2630/10/4/043020.

[8] R. Zhu, X.N. Liu, G.K. Hu, C.T. Sun, G.L. Huang, Negative refraction of elastic waves at the deep-subwavelength scale in a single-phase metamaterial, Nature Commun. 5 (1) (2014) 5510, http://dx.doi.org/10.1038/ncomms6510.

[9] N. Fang, D. Xi, J. Xu, M. Ambati, W. Srituravanich, C. Sun, X. Zhang, Ultrasonic metamaterials with negative modulus, Nature Mater. 5 (6) (2006) 452–456, http://dx.doi.org/10.1038/nmat1644.

[10] S.H. Lee, C.M. Park, Y.M. Seo, Z.G. Wang, C.K. Kim, Acoustic metamaterial with negative modulus, J. Phys.: Condens. Matter 21 (17) (2009) 175704, http://dx.doi.org/10.1088/0953-8984/21/17/175704.

[11] Z. Liu, X. Zhang, Y. Mao, Y.Y. Zhu, Z. Yang, C.T. Chan, P. Sheng, Locally resonant sonic materials, Science 289 (5485) (2000) 1734–1736, http://dx.doi.org/10.1126/science.289.5485.1734, arXiv:https://science.sciencemag.org/content/289/5485/1734.full.pdf, URL https://science.sciencemag.org/content/289/5485/1734.

[12] D. Torrent, J. Sánchez-Dehesa, Anisotropic mass density by two-dimensional acoustic metamaterials, New J. Phys. 10 (2) (2008) 023004, http://dx.doi.org/10.1088/1367-2630/10/2/023004.

[13] Y. Ding, Z. Liu, C. Qiu, J. Shi, Metamaterial with simultaneously negative bulk modulus and mass density, Phys. Rev. Lett. 99 (2007) 093904, http://dx.doi.org/10.1103/PhysRevLett.99.093904, URL https://link.aps.org/doi/10.1103/PhysRevLett.99.093904.

[14] F. Liu, X. Huang, C.T. Chan, Dirac cones at k=0 in acoustic crystals and zero refractive index acoustic materials, Appl. Phys. Lett. 100 (7) (2012) 071911, http://dx.doi.org/10.1063/1.3686907.

[15] X. Zhang, Z. Liu, Negative refraction of acoustic waves in two-dimensional phononic crystals, Appl. Phys. Lett. 85 (2) (2004) 341–343, http://dx.doi.org/10.1063/1.1772854.

[16] R.V. Craster, S. Guenneau, Acoustic Metamaterials: Negative Refraction, Imaging, Lensing and Cloaking, Vol. 166, Springer Science & Business Media, 2012.

[17] M. Ambati, N. Fang, C. Sun, X. Zhang, Surface resonant states and superlensing in acoustic metamaterials, Phys. Rev. B 75 (2007) 195447, http://dx.doi.org/10.1103/PhysRevB.75.195447, URL https://link.aps.org/doi/10.1103/PhysRevB.75.195447.

[18] H. Zhang, X. Zhou, G. Hu, Shape-adaptable hyperlens for acoustic magnifying imaging, Appl. Phys. Lett. 109 (22) (2016) 224103, http://dx.doi.org/10.1063/1.4971364.

[19] H. Chen, C.T. Chan, Acoustic cloaking and transformation acoustics, J. Phys. D: Appl. Phys. 43 (11) (2010) 113001, http://dx.doi.org/10.1088/0022-3727/43/11/113001.

[20] Y. Chen, X. Liu, G. Hu, Latticed pentamode acoustic cloak, Sci. Rep. 5 (1) (2015) 15745, http://dx.doi.org/10.1038/srep15745.

[21] J.R. Willis, Variational principles for dynamic problems for inhomogeneous elastic media, Wave Motion 3 (1) (1981) 1–11, http://dx.doi.org/10.1016/0165-2125(81)90008-1, URL https://www.sciencedirect.com/science/article/pii/0165212581900081.

[22] H. Nassar, Q.-C. He, N. Auffray, Willis elastodynamic homogenization theory revisited for periodic media, J. Mech. Phys. Solids 77 (2015) 158–178, http://dx.doi.org/10.1016/j.jmps.2014.12.011, URL https://www.sciencedirect.com/science/article/pii/S0022509614002579.

[23] C.F. Sieck, A. Alù, M.R. Haberman, Origins of Willis coupling and acoustic bianisotropy in acoustic metamaterials through source-driven homogenization, Phys. Rev. B 96 (2017) 104303, http://dx.doi.org/10.1103/PhysRevB.96.104303, URL https://link.aps.org/doi/10.1103/PhysRevB.96.104303.

[24] M.B. Muhlestein, C.F. Sieck, P.S. Wilson, M.R. Haberman, Experimental evidence of Willis coupling in a one-dimensional effective material element, Nature Commun. 8 (1) (2017) 15625, http://dx.doi.org/10.1038/ncomms15625.

[25] S. Koo, C. Cho, J.-h. Jeong, N. Park, Acoustic omni meta-atom for decoupled access to all octants of a wave parameter space, Nature Commun. 7 (1) (2016) 13012, http://dx.doi.org/10.1038/ncomms13012.

[26] J. Li, C. Shen, A. Díaz-Rubio, S.A. Tretyakov, S.A. Cummer, Systematic design and experimental demonstration of bianisotropic metasurfaces for scattering-free manipulation of acoustic wavefronts, Nature Commun. 9 (1) (2018) 1342, http://dx.doi.org/10.1038/s41467-018-03778-9.

[27] S.R. Craig, X. Su, A. Norris, C. Shi, Experimental realization of acoustic bianisotropic gratings, Phys. Rev. Appl. 11 (2019) 061002, http://dx.doi.org/10.1103/PhysRevApplied.11.061002, URL https://link.aps.org/doi/10.1103/PhysRevApplied.11.061002.

[28] H. Esfahlani, Y. Mazor, A. Alù, Homogenization and design of acoustic Willis metasurfaces, Phys. Rev. B 103 (2021) 054306, http://dx.doi.org/10.1103/PhysRevB.103.054306, URL https://link.aps.org/doi/10.1103/PhysRevB.103.054306.

[29] Y. Zhai, H.-S. Kwon, B.-I. Popa, Active Willis metamaterials for ultracompact nonreciprocal linear acoustic devices, Phys. Rev. B 99 (2019) 220301, http://dx.doi.org/10.1103/PhysRevB.99.220301, URL https://link.aps.org/doi/10.1103/PhysRevB.99.220301.

[30] Y. Chen, X. Li, G. Hu, M.R. Haberman, G. Huang, An active mechanical Willis meta-layer with asymmetric polarizabilities, Nature Commun. 11 (1) (2020) 3681, http://dx.doi.org/10.1038/s41467-020-17529-2.

[31] L. Rayleigh, On waves propagated along the plane surface of an elastic solid, Proc. Lond. Math. Soc. s1-17 (1) (1885) 4–11, http://dx.doi.org/10.1112/plms/s1-17.1.4, arXiv:https://londmathsoc.onlinelibrary.wiley.com/doi/pdf/10.1112/plms/s1-17.1.4, URL https://londmathsoc.onlinelibrary.wiley.com/doi/abs/10.1112/plms/s1-17.1.4.

[32] R. Stoneley, H.F. Baker, Elastic waves at the surface of separation of two solids, Proc. R. Soc. Lond. Ser. A Contain. Pap. Math. Phys. Charact. 106 (738) (1924) 416–428, http://dx.doi.org/10.1098/rspa.1924.0079, arXiv:https://royalsocietypublishing.org/doi/pdf/10.1098/rspa.1924.0079, URL https://royalsocietypublishing.org/doi/abs/10.1098/rspa.1924.0079.

[33] J.G. Scholte, The range of existence of Rayleigh and Stoneley waves, Geophys. Suppl. Mon. Not. R. Astron. Soc. 5 (5) (1947) 120–126, http://dx.doi.org/10.1111/j.1365-246X.1947.tb00347.x, arXiv:https://academic.oup.com/gsmnras/article-pdf/5/5/120/1469979/5-5-120.pdf.

[34] Y.I. Bobrovnitskii, A Rayleigh-type wave at the plane interface of two homogeneous fluid half-spaces, Acoust. Phys. 57 (5) (2011) 595, http://dx.doi.org/10.1134/S1063771011050046.

[35] S.P. Wallen, C.F. Sieck, B.M. Goldsberry, M.D. Guild, G. Orris, M.R. Haberman, Guided waves at bianisotropic fluid interfaces, J. Acoust. Soc. Am. 144 (3) (2018) 1832, http://dx.doi.org/10.1121/1.5068071.

[36] M.B. Muhlestein, C.F. Sieck, A. Alù, M.R. Haberman, Reciprocity, passivity and causality in Willis materials, Proc. R. Soc. A Math. Phys. Eng. Sci. 472 (2194) (2016) 20160604, http://dx.doi.org/10.1098/rspa.2016.0604, arXiv:https://royalsocietypublishing.org/doi/pdf/10.1098/rspa.2016.0604, URL https://royalsocietypublishing.org/doi/abs/10.1098/rspa.2016.0604.

[37] M.B. Muhlestein, B.M. Goldsberry, A.N. Norris, M.R. Haberman, Acoustic scattering from a fluid cylinder with Willis constitutive properties, Proc. R. Soc. A Math. Phys. Eng. Sci. 474 (2220) (2018) 20180571, http://dx.doi.org/10.1098/rspa.2018.0571, arXiv:https://royalsocietypublishing.org/doi/pdf/10.1098/rspa.2018.0571, URL https://royalsocietypublishing.org/doi/abs/10.1098/rspa.2018.0571.

[38] B.-I. Popa, S.A. Cummer, Complex coordinates in transformation optics, Phys. Rev. A 84 (2011) 063837, http://dx.doi.org/10.1103/PhysRevA.84.063837, URL https://link.aps.org/doi/10.1103/PhysRevA.84.063837.

[39] Z. Chang, D. Guo, X.-Q. Feng, G. Hu, A facile method to realize perfectly matched layers for elastic waves, Wave Motion 51 (7) (2014) 1170–1178, http://dx.doi.org/10.1016/j.wavemoti.2014.07.003, URL https://www.sciencedirect.com/science/article/pii/S0165212514000869.

[40] A. Melnikov, Y.K. Chiang, L. Quan, S. Oberst, A. Alù, S. Marburg, D. Powell, Acoustic meta-atom with experimentally verified maximum Willis coupling, Nature Commun. 10 (1) (2019) 3148, http://dx.doi.org/10.1038/s41467-019-10915-5.